Modeling and Analysis of Driving Behavior Based on a Probability-Weighted ARX Model

Hiroyuki Okuda, Norimitsu Ikami, Tatsuya Suzuki, *Member, IEEE*, Yuichi Tazaki, *Member, IEEE*, and Kazuya Takeda, *Senior Member, IEEE*

***Abstract*—This paper proposes a probability-weighted autoregressive exogenous (PrARX) model wherein the multiple ARX models are composed of the probabilistic weighting functions. This model can represent both the motion-control and decision-making aspects of the driving behavior. As the probabilistic weighting function, a "softmax" function is introduced. Then, the parameter estimation problem for the proposed model is formulated as a single optimization problem. The "soft" partition defined by the PrARX model can represent the decision-making characteristics of the driver with vagueness. This vagueness can be quantified by introducing the "decision entropy." In addition, it can be easily extended to the online estimation scheme due to its small computational cost. Finally, the proposed model is applied to the modeling of the vehicle-following task, and the usefulness of the model is verified and discussed.**

***Index Terms*—Decision entropy, driver model, identification, probability-weighted autoregressive exogenous (PrARX) model.**

I. Introduction

RECENTLY, an individualized driver-assisting system has been attracting much attention to realize personalized safety driving. A quantitative and rigorous mathematical model, which can express the dynamical characteristics of the driving behavior, is required to realize such an individualized driver-assisting system.

Many ideas have been exploited for the driving behavior modeling from the viewpoint of control technology [1]–[6]. The common idea in these studies is that the driver is regarded as a kind of "controller," and linear control theory has been applied to analyze the driving behavior. The linear controller model, however, may not work in the case where the driver is requested to operate the vehicle using not only simple reflexive motion but higher level decision-making as well. On the other hand, a nonlinear and/or stochastic modeling of human behavior such as neural networks and hidden Markov models (HMM) has been developed [7]–[10]. These techniques, however, have some problems, particularly when some applications are considered. For example, it may be difficult to estimate the driver's physical and mental state from these models, and the usefulness of information obtained by these models also remains questionable for the design of a driver-assisting system.

When we look at the human behavior, it is often found that the driver appropriately switches the simple control laws instead of adopting the complex nonlinear control law [11]–[13]. This idea can be formally formulated by introducing so-called "hybrid systems" (HSs) wherein the switching among modes are represented by the discrete-event-driven system, whereas the dynamics of each mode are characterized by the continuous-time-driven system. Furthermore, the switching mechanism (mode segmentation) can be regarded as a kind of driver's decision-making in the complex task. Thus, the introduction of the HS model leads to higher level understanding of the human behavior wherein the motion-control and decision-making aspects are synthesized. The simultaneous understanding of decision-making and motion control must be useful, particularly when we consider the classification of drivers. For example, the driver who has good performance in motion control but bad performance in decision-making is regarded as a "hasty" driver and is likely to cause a serious accident.

In the hybrid system identification, a piecewise affine autoregressive exogenous (PWARX) model is widely used as the mathematical model. Many identification algorithms for the PWARX model have been proposed [14]–[18]. The main concern in the hybrid system identification is how to identify the parameters in the ARX models and the coefficients in the hyperplanes defining the partition between modes in the regressor space.

We already have investigated the effectiveness of the HS modeling of the human driving behavior [20]–[22]. In [21], the driving behavior was successfully analyzed from the viewpoint of HSs using the piecewise linear model and mixed integer programming (MIP). However, this paper addressed a short-term (small data set) task focusing on the collision-avoidance behavior due to high computational cost in the MIP. In [21], the standard HMM was extended to the stochastic switched ARX model by embedding an ARX model into each discrete state. Although this model can be a powerful tool for behavior recognition, the mode-switching mechanism is specified based only on the constant mode transition probability and is not characterized by the regressor variables at all. This may be a significant drawback when we try to analyze the decision-making aspect of the driver. In [22], the vehicle-following

Manuscript received November 1, 2011; revised March 12, 2012 and June 4, 2012; accepted June 13, 2012. Date of publication August 1, 2012; date of current version February 25, 2013. This work was supported in part by the Japan Science and Technology Agency Core Research for Evolutional Science and Technology Japan. The Associate Editor for this paper was C. Wu.

The authors are with Nagoya University, Nagoya 464-8603, Japan (e-mail: h_okuda@nuem.nagoya-u.ac.jp).

Color versions of one or more of the figures in this paper are available online at http://ieeexplore.ieee.org.

Digital Object Identifier 10.1109/TITS.2012.2207893

task was analyzed by the PWARX model, together with the clustering-based identification scheme [14]. The obtained results were quite interesting in a sense that the motion-control and decision-making aspects were simultaneously captured. However, in the clustering-based scheme, the data classification (mode assignment) is executed first; then, estimation of the parameters in the ARX models and of the coefficients in the partitioning hyperplanes are sequentially executed. Due to this two-stage identification, this identification scheme leads to high computational cost, and it may be hard to execute this identification scheme online. In addition, the PWARX model cannot explicitly express the "mixed mode" that represents the overlapping between modes and plays an essential role in the analysis of the decision-making characteristics in the human behavior.

In this paper, first of all, a probability-weighted ARX (PrARX) model, wherein the multiple ARX models are composed by the probabilistic weighting function, is proposed. This model is obtained by embedding the "softmax function" in the expression of the partition instead of the deterministic partition used in the PWARX model. The partition is characterized by the parameters in the softmax function in the PrARX model. Then, the parameter-estimation problem for the PrARX model is addressed. The parameter-estimation problem for the ARX models and the softmax functions is formulated as a single optimization problem due to the continuity of the softmax function. Furthermore, the identified PrARX model can be easily transformed in to the corresponding PWARX model wherein the complete deterministic partition is defined by the parameters in the softmax functions.

Generally speaking, the dynamical characteristics of the driving behavior may change due to various reasons, such as gaining experience, fatigue, change of driving conditions, and so on. If the parameters in the driving behavior model were assumed to be constant, there is a great possibility that the accuracy of the model degrades over time. Since the performance of the individualized driver-assisting system is directly influenced by the accuracy of the driving behavior model, it is of critical importance to frequently update the model so that it can always express the driving behavior with enough accuracy. One of the advantages of the PrARX model is that the parameter estimation can be executed in an adaptive manner due to its simple parameter-estimation algorithm with small computational cost. Therefore, we develop an adaptive parameter-estimation scheme for the PrARX model, which can update the estimated parameters online and, as a result, can adapt to the change in the driving characteristics.

Based on these theoretical developments, the PrARX model is applied to the modeling of the driving behavior, particularly focusing on the vehicle-following task. The driving characteristics are quantified from both the motion-control and decision-making aspects. In addition, since the PrARX model can express the stochastic variance of the mode segmentation, i.e., the decision-making, it can be used to quantify a "decision entropy" in the human behavior. Finally, the usefulness of the adaptive parameter-estimation scheme is also demonstrated through some numerical examples and driving data analysis.

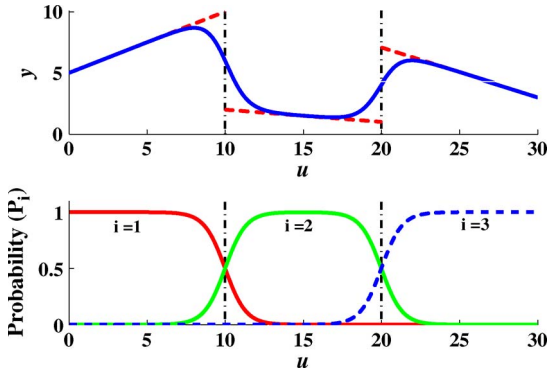

Fig. 1. Sample model of the single-output PrARX model with three modes.

II. PrARX Model

A. Definition of the Model

We propose a PrARX model wherein the multiple ARX models are composed of the probabilistic weighting functions. The PrARX model is defined by the following form:

$$\boldsymbol{y}_k = f_{\mathrm{PrARX}}(\boldsymbol{r}_k) + \boldsymbol{e}_k \tag{1}$$

where $k \geq 0$ denotes the sampling index, $\boldsymbol{y} \in \mathbb{R}^q$ is the output variable, and $\boldsymbol{e}_k$ is an error term. $\boldsymbol{r}_k$ is a regressor vector defined by

$$\boldsymbol{r}_k = \left[\boldsymbol{y}_{k-1}^T \ \cdots \ \boldsymbol{y}_{k-n_a}^T \ \boldsymbol{u}_{k-1}^T \ \cdots \ \boldsymbol{u}_{k-n_b}^T\right]^T \tag{2}$$

where $\boldsymbol{r}_k \in \mathbb{R}^n$, with $n = p \cdot n_a + q \cdot n_b$, and $\boldsymbol{u} \in \mathbb{R}^p$ is the input variable. n_a and n_b are the orders of the ARX model. $f_{\mathrm{PrARX}}(\boldsymbol{r}_k)$ is a function of the following form:

$$f_{\mathrm{PrARX}}(\boldsymbol{r}_k) = \sum_{i=1}^{s} P_i \boldsymbol{\theta}_i^T \boldsymbol{\varphi}_k \tag{3}$$

where $\boldsymbol{\varphi}_k = [\boldsymbol{r}_k^T \ 1]^T \in \mathbb{R}^{n+1}$. $\boldsymbol{\theta}_i \in \mathbb{R}^{(n+1)\times q}$ $(i = 1, \ldots, s)$ is an unknown parameter matrix of each mode. s is the number of modes and is supposed to be known. P_i denotes the probability that the corresponding regressor vector $\boldsymbol{r}_k$ belongs to the mode i and is given by the softmax function as follows:

$$\begin{aligned} P_i &= \frac{\exp\left(\boldsymbol{\eta}_i^T \boldsymbol{\varphi}_k\right)}{\sum_{j=1}^{s} \exp\left(\boldsymbol{\eta}_j^T \boldsymbol{\varphi}_k\right)} \\ \boldsymbol{\eta}_s &= \boldsymbol{0} \end{aligned} \tag{4}$$

where $\boldsymbol{\eta}_i$ $(i = 1, \ldots, s-1)$ is an unknown parameter that characterizes the probabilistic partition between regions corresponding to each mode.

The sample model is shown in Fig. 1. This model is the single-output PrARX model with three modes. The model parameters are given by

$$\begin{aligned} \theta_1 &= [0.5 \quad -5]^T \\ \theta_2 &= [-0.1 \quad 3]^T \\ \theta_3 &= [-0.4 \quad 15]^T \\ \eta_1 &= [-3 \quad 45]^T \\ \eta_2 &= [-1.5 \quad 30]^T \\ \eta_3 &= [0 \quad 0]^T. \end{aligned} \tag{5}$$

It can be seen that the three ARX models are smoothly connected at $u = 10$ and 20. These connecting points, i.e., the partitions, can be calculated from the η_1 and η_2 (see Section II-C).

B. Identification Algorithm

To identify the parameters in the PrARX model, the steepest descent method is used. The cost function is defined as the square norm of the output error as follows:

$$\epsilon = \frac{1}{N}\sum_{k=1}^{N}\|\boldsymbol{e}_k\|^2 = \frac{1}{N}\sum_{k=1}^{N}\boldsymbol{e}_k^T\boldsymbol{e}_k \tag{6}$$

where N is the number of data. Then, the partial differentiation of the objective function is given as follows:

$$\frac{\partial\epsilon}{\partial\boldsymbol{\theta}_i} = -\frac{1}{N}\sum_{k=1}^{N}2P_i\boldsymbol{\varphi}_k\boldsymbol{e}_k^T \tag{7}$$

$$\frac{\partial\epsilon}{\partial\boldsymbol{\eta}_i} = -\frac{1}{N}\sum_{k=1}^{N}2P_i\boldsymbol{\varphi}_k\boldsymbol{e}_k^T\left(\boldsymbol{\theta}_i\boldsymbol{\varphi}_k - f_{\mathrm{PrARX}}(\boldsymbol{r}_k)\right). \tag{8}$$

The minimization of the cost function is obtained by updating the parameters in the steepest descent direction as follows:

$$\boldsymbol{\theta}_i^{(t+1)} = \boldsymbol{\theta}_i^{(t)} - \boldsymbol{\alpha}\frac{\partial\epsilon^{(t)}}{\partial\boldsymbol{\theta}_i^{(t)}} \tag{9}$$

$$\boldsymbol{\eta}_i^{(t+1)} = \boldsymbol{\eta}_i^{(t)} - \boldsymbol{\beta}\frac{\partial\epsilon^{(t)}}{\partial\boldsymbol{\eta}_i^{(t)}} \tag{10}$$

where $\boldsymbol{\theta}_i^{(t)}$, $\boldsymbol{\eta}_i^{(t)}$, and $\epsilon^{(t)}$ are updated parameters and the cost functions at the tth iteration. α and β are small positive numbers.

Remark 2.1: The parameters $\boldsymbol{\theta}_i$ in the ARX models and $\boldsymbol{\eta}_i$ in the partitions of the regions (softmax function) can be simultaneously optimized by the single optimization.

Remark 2.2: The amount of computation in (7) and (8) grows in proportion to the number of data N (neither exponential nor polynomial order).

Remark 2.3: Although the parameter-estimation results are affected by the setting of the initial parameter, several offline identification schemes such as a clustering-based approach [14], [15] can be exploited to specify the good initial parameter in the estimation algorithm.

C. Transformation to the PWARX Model

The proposed PrARX model can be easily transformed to the corresponding PWARX model with complete partition. The transformation rule from the PrARX model to the PWARX model is discussed here.

1) PWARX Model: The PWARX model is defined by the following form:

$$\boldsymbol{y}_k = f_{\mathrm{PWARX}}(\boldsymbol{r}_k) + \boldsymbol{e}_k. \tag{11}$$

$f_{\mathrm{PWARX}}(\boldsymbol{r}_k)$ is a PWA function of the following form:

$$f_{\mathrm{PWARX}}(\boldsymbol{r}_k) = \begin{cases} \boldsymbol{\theta}_1^T\boldsymbol{\varphi}_k & \text{if } \boldsymbol{r}_k \in \mathcal{R}_1 \\ \vdots & \vdots \\ \boldsymbol{\theta}_s^T\boldsymbol{\varphi}_k & \text{if } \boldsymbol{r}_k \in \mathcal{R}_s \end{cases} \tag{12}$$

where $\{\mathcal{R}_i\}_{i=1}^s$ gives a complete partition of the regressor domain $\mathcal{R} \subseteq \mathbb{R}^n$. Each region $\mathcal{R}_i$ is a convex polyhedron described by

$$\mathcal{R}_i = \left\{\boldsymbol{r} \in \mathbb{R}^n : \boldsymbol{H}_i\boldsymbol{\varphi} \preceq_{[i]} \boldsymbol{0}\right\} \tag{13}$$

where $\boldsymbol{H}_i$ is a matrix that defines the partition $\{\mathcal{R}_i\}_{i=1}^s$. The symbol $\preceq_{[i]}$ denotes a vector whose elements can be the symbols $\leq$ or $<$.

2) Transformation to PWARX from the PrARX *Model:* Consider the assignment of each $\boldsymbol{r}_k$ to the mode i using the following rule:

$$\boldsymbol{r}_k \in \mathcal{R}_i \quad i = \underset{i=1,\ldots,s}{\arg\max}\, P_i. \tag{14}$$

This mode assignment implies that the $\{\mathcal{R}_i\}_{i=1}^s$ is represented by using $\boldsymbol{\eta}_i$ values as follows:

$$\mathcal{R}_i = \left\{\boldsymbol{r} \in \mathbb{R}^n : \boldsymbol{H}_i\boldsymbol{\varphi} \preceq_{[i]} \boldsymbol{0}\right\} \tag{15}$$

$$\boldsymbol{H}_i = \left[(\boldsymbol{\eta}_1 - \boldsymbol{\eta}_i)\cdots(\boldsymbol{\eta}_s - \boldsymbol{\eta}_i)\right]^T. \tag{16}$$

Theorem 2.1: $\{\mathcal{R}_i\}_{i=1}^s$ given by (15) and (16) is a complete partition of $\mathbb{R}^n$, i.e.,

$$\mathcal{R}_1 \cup \cdots \cup \mathcal{R}_s = \mathbb{R}^n \tag{17}$$

$$\mathcal{R}_l \cap \mathcal{R}_m = \phi \quad {}^\forall l, \quad {}^\forall m, \quad l \neq m. \tag{18}$$

Proof: P_i can be calculated for any $\boldsymbol{r} \in \mathbb{R}^n$ by (4). $\boldsymbol{r}$ always belongs to one of the areas $\{\mathcal{R}\}_{i=1}^s$. Therefore, $\mathcal{R}_1 \cup \cdots \cup \mathcal{R}_s = \mathbb{R}^n$ is obvious.

Next, consider the intersection $\mathcal{R}_l \cap \mathcal{R}_m$ for any l and m, i.e.,

$$\boldsymbol{H}_l = \left[(\boldsymbol{\eta}_1 - \boldsymbol{\eta}_l)\cdots(\boldsymbol{\eta}_m - \boldsymbol{\eta}_l)\cdots(\boldsymbol{\eta}_s - \boldsymbol{\eta}_l))\right]^T \tag{19}$$

$$\boldsymbol{H}_m = \left[(\boldsymbol{\eta}_1 - \boldsymbol{\eta}_m)\cdots(\boldsymbol{\eta}_l - \boldsymbol{\eta}_m)\cdots(\boldsymbol{\eta}_s - \boldsymbol{\eta}_m))\right]^T. \tag{20}$$

For $\boldsymbol{H}_l$ and $\boldsymbol{H}_m$

$$\left\{(\boldsymbol{\eta}_m - \boldsymbol{\eta}_l)^T\boldsymbol{\varphi} \leq \boldsymbol{0}\right\} \cap \left\{(\boldsymbol{\eta}_l - \boldsymbol{\eta}_m)^T\boldsymbol{\varphi} \leq \boldsymbol{0}\right\} = \phi \tag{21}$$

always holds. Therefore

$$\mathcal{R}_l \cap \mathcal{R}_m = \phi. \tag{22}$$

As the consequence, $\{\mathcal{R}_i\}_{i=1}^s$ is the complete partition of the $\mathbb{R}^n$. ■

Due to this theorem, the PrARX model can be directly transformed into the PWARX model by simply applying (16) to the identified PrARX model. Note that no transformation is necessary for θ_i values.

D. Numerical Experiments

1) Example 1: Let the data $\{(u_{k-1}, y_k)\}_{k=1}^{100}$ be generated by a system given by

$$\begin{aligned} y_k &= f_{\mathrm{PrARX}}(u_{k-1}) + e_k \\ \theta_1 &= [1 \quad -0.5]^T \\ \theta_2 &= [-2 \quad 1.5]^T \\ \boldsymbol{\eta}_1 &= [-20 \quad 10]^T \\ \boldsymbol{\eta}_2 &= [0 \quad 0]^T \end{aligned} \tag{23}$$

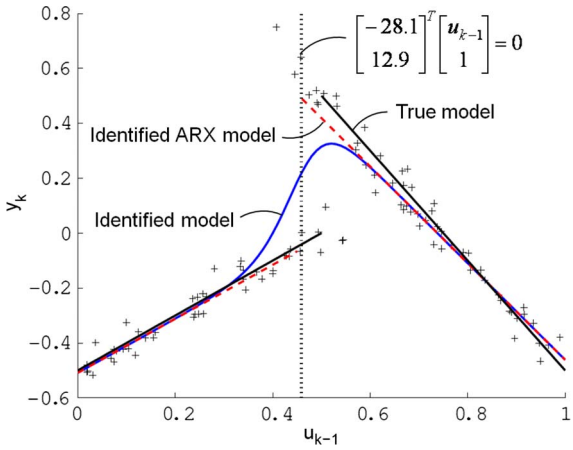

Fig. 2. Identification of the PrARX model with two modes. True ARX models (black solid lines), an identified PrARX model (blue solid line), identified ARX models (red dashed lines), mode partition (vertical black dashed line), and the data set used for identification are shown.

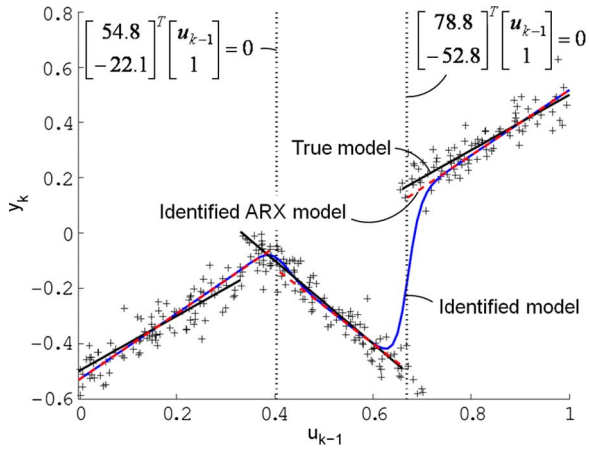

Fig. 3. Identification of the PrARX model with three modes wherein two modes have the same ARX parameters. True ARX models (black solid lines), identified PrARX models (blue solid line), identified ARX models (red dashed lines), mode partition (vertical black dashed line), and the data set used for identification are shown.

where e_k is a sequence of the normally distributed random numbers with zero mean and variance $\sigma_e^2 = 0.025$. In Fig. 2, two true ARX models (depicted by two red dashed lines), the identified model (depicted by a blue solid line), and the data set used for the identification (depicted by " + " marks) are shown. The partition among modes is also designated by the vertical black dashed line. The estimated parameters are

$$\theta_1 = [0.98 \quad -0.51]^T, \quad \theta_2 = [-1.76 \quad 1.30]^T$$
$$\eta_1 = [-28.1 \quad 12.9]^T, \quad \eta_2 = [0 \quad 0]^T.$$

From this example, it can be confirmed that the identification of the PrARX model works well. Then, by applying the rule (16), we get

$$\boldsymbol{H}_1 = \left[[0 \quad 0]^T \quad [28.1 \quad -12.9]^T\right]^T \tag{24}$$
$$\boldsymbol{H}_2 = \left[[-28.1 \quad 12.9]^T \quad [0 \quad 0]^T\right]^T. \tag{25}$$

Therefore, the deterministic partition between modes 1 and 2 is given by

$$[\,-28.1 \quad 12.9\,]\begin{bmatrix}u_{k-1}\\1\end{bmatrix} = \mathbf{0}. \tag{26}$$

(In this example, the partition is specified only by the η_1.)

2) Example 2: Let the data $\{(u_{k-1}, y_k)\}_{k=1}^{300}$ be generated by a system given by

$$\begin{aligned} y_k &= f_{\mathrm{PrARX}}(u_{k-1}) + e_k \\ \theta_1 &= [1 \quad -0.5]^T \\ \theta_2 &= [-1.5 \quad 0.5]^T \\ \theta_3 &= [1 \quad -0.5]^T \\ \boldsymbol{\eta}_1 &= [120 \quad 60]^T \\ \boldsymbol{\eta}_2 &= [-60 \quad 40]^T \\ \boldsymbol{\eta}_3 &= [0 \quad 0]^T \end{aligned} \tag{27}$$

where e_k is a sequence of the normally distributed random numbers with zero mean and a variance $\sigma_e^2 = 0.025$. In this example, although modes 1 and 3 have the same ARX parameters $\boldsymbol{\theta}_i$, they are expressed as the different modes because they are located on different regions. The region of mode 2 is located between the regions of modes 1 and 3. The true model, the identified model, and the data set used for identification are shown in Fig. 3. From this figure, it can be confirmed that modes 1 and 3 can be successfully identified as the different modes. The estimated parameters are

$$\begin{aligned} \theta_1 &= [1.20 \quad -0.53]^T \\ \theta_2 &= [-1.36 \quad 0.42]^T \\ \theta_3 &= [1.18 \quad -0.66]^T \\ \eta_1 &= [-133.6 \quad 74.9]^T \\ \eta_2 &= [-78.8 \quad 52.8]^T \\ \eta_3 &= [0 \quad 0]^T. \end{aligned} \tag{28}$$

Then, by applying (16), we get

$$\boldsymbol{H}_1 = \left[[0\,0]^T\ [54.8 \ -22.1]^T\ [133.6 \ -74.9]^T\right]^T \tag{29}$$
$$\boldsymbol{H}_2 = \left[[-54.8\ 22.1]^T\ [0\,0]^T\ [78.8 \ -52.8]^T\right]^T \tag{30}$$
$$\boldsymbol{H}_3 = \left[[-133.6\ 74.9]^T\ [-78.8\ 52.8]^T\ [0\,0]^T\right]^T. \tag{31}$$

Therefore, the deterministic partition between modes 1 and 2 is given by

$$[\,54.8 \quad -22.1\,]\begin{bmatrix}u_{k-1}\\1\end{bmatrix} = \mathbf{0}. \tag{32}$$

Similarly, the partition between modes 2 and 3 is given by

$$[\,78.8 \quad -52.8\,]\begin{bmatrix}u_{k-1}\\1\end{bmatrix} = \mathbf{0}. \tag{33}$$

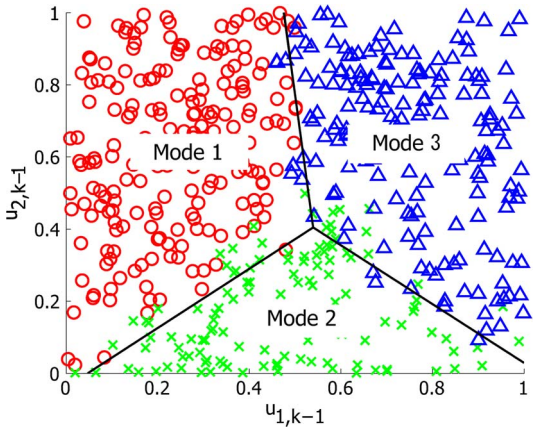

Fig. 4. Identified partitions and classification of data. (◯, ×, and △ represent the data points assigned to modes 1, 2, and 3, respectively.)

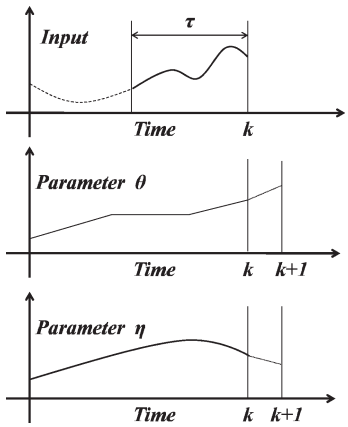

Fig. 5. Illustration of data length τ.

3) Example 3: Let the data $\{(u_{1,k-1}, u_{2,k-1}, y_k)\}_{k=1}^{500}$ be generated by a system given by

$$\begin{aligned} y_k &= f_{\mathrm{PrARX}}\left([u_{1,k-1}, u_{2,k-1}]^T\right) + e_k \\ \theta_1 &= [5 \quad -4 \quad -3]^T \\ \theta_2 &= [6 \quad 3 \quad -6]^T \\ \theta_3 &= [-3 \quad 5 \quad 0]^T \\ \eta_1 &= [-30 \quad 0 \quad 15]^T \\ \eta_2 &= [-15 \quad -15 \quad 15]^T \\ \eta_3 &= [0 \quad 0 \quad 0]^T \end{aligned} \tag{34}$$

where e_k is a sequence of the normally distributed random numbers with zero mean and variance $\sigma_e^2 = 0.025$. The estimated parameters are

$$\begin{aligned} \theta_1 &= [3.98 \quad -4.23 \quad -2.729]^T \\ \theta_2 &= [6.18 \quad 1.78 \quad -6.00]^T \\ \theta_3 &= [-3.46 \quad 4.84 \quad 0.50]^T \\ \eta_1 &= [-23.95 \quad 0.42 \quad 11.42]^T \\ \eta_2 &= [-11.48 \quad -10.56 \quad 11.24]^T \\ \eta_3 &= [0 \quad 0 \quad 0]^T. \end{aligned} \tag{35}$$

The parameters in the hyperplane in the corresponding PWARX model are obtained from η_i by applying (16), similar to examples 1 and 2. The obtained hyperplane parameters are

$$H_1 = \begin{bmatrix} 0 & 0 & 0 \\ 12.47 & -10.98 & -0.18 \\ 23.95 & -0.42 & -11.42 \end{bmatrix} \tag{36}$$

$$H_2 = \begin{bmatrix} -12.47 & 10.98 & 0.18 \\ 0 & 0 & 0 \\ 11.48 & 10.56 & -11.24 \end{bmatrix} \tag{37}$$

$$H_3 = \begin{bmatrix} -23.95 & 0.42 & 11.42 \\ -11.48 & -10.56 & 11.24 \\ 0 & 0 & 0 \end{bmatrix}. \tag{38}$$

The data set used for identification and the partitions calculated from estimated η_i values are shown in Fig. 4. In Fig. 4, ◯, ×, and △ represent modes 1, 2, and 3, respectively, assigned to data by applying (14). In addition, the partitions among modes are shown by a black solid line in the figure. From this figure, it can be confirmed that the complete partition is realized.

E. Adaptive Parameter Estimation of the PrARX *Model*

The parameter-estimation method for the PrARX model presented earlier is an offline method, i.e., enough input/output data are collected first, and then the parameters are estimated. In application to human behavior modeling, however, the behavioral characteristics of the motion control and the decision-making may vary due to the effect of accommodation with the task, slight change of the interface, and the driver's fatigue. For the realization of a system that better assists drivers based on the driving behavior model, an adaptive parameter-estimation scheme that can deal with such change of the behavior should be exploited. Here, the adaptive parameter-estimation method for the PrARX model is developed. As described earlier, the optimal parameters of the PrARX model can be estimated in the steepest descent manner by sufficiently using many initial parameters. In the case of online estimation, however, the parameters must be updated within the allotted computation time. Thus, it is almost impossible to test many initial parameters at every sampling instant to obtain the globally optimal set of parameters.

To relax the problem, we make an assumption that human driving behavior does not exhibit an abrupt change in its dynamical characteristics, i.e., it changes gradually with sufficiently slow speed. This assumption justifies the use of the optimal parameters obtained at the kth sampling instant as the initial parameters for the $(k+1)$th sampling instant. In this way, we can track the change of the model parameters under strict time constraints.

1) Procedure of Adaptive Estimation: The adaptive parameter estimation is executed in the following procedure (see Fig. 5). Here, the estimated model parameters at the kth sampling instant are denoted by θ_k and η_k.

Step 1: Set k to be 0, and set initial estimated parameters to be θ_0 and η_0.

Step 2: Acquire τ steps of input/output data $\phi_{k-\tau}, \ldots, \phi_k$, where τ denotes the length of data used for parameter estimation.

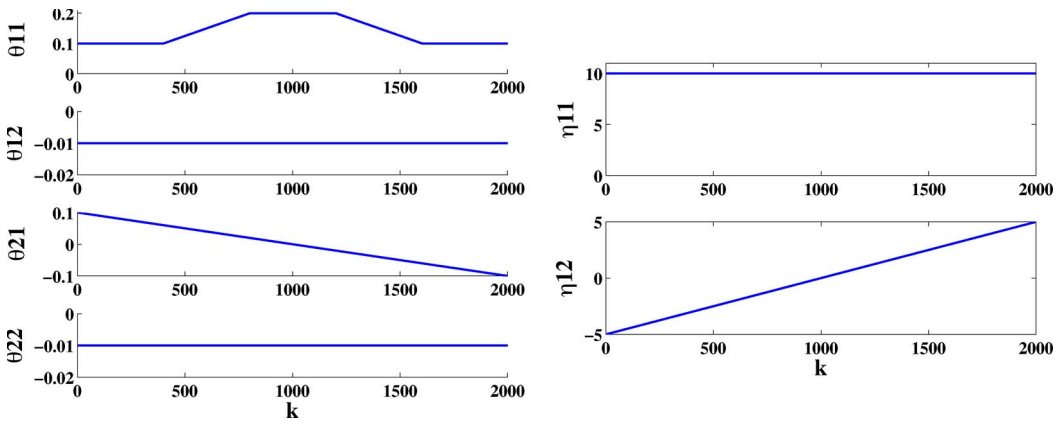

Fig. 6. Profiles of parameters in the test model.

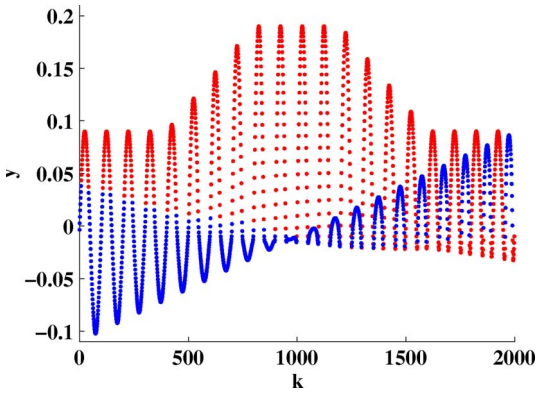

Fig. 7. Output signal of the test model (plotted in red when $P_1(\phi_k) \geq P_2(\phi_k)$ and in blue if otherwise).

Step 3: Using τ steps of data, estimate optimal parameters θ_{k+1} and η_{k+1} by using (9) and (10) with setting N to be τ. The initial estimated parameters are set to be θ_k and η_k. Note that the number of iterations in (9) and (10) is restricted to 200 in the adaptive version due to the strict time constraints. (The sampling interval is set to be 200 ms in our application to the driving data.)

Step 4: Increase k by 1, and go to step 2.

2) Numerical Example: Here, the proposed method is verified using data generated by an artificial model (see Fig. 6) whose pattern of parameter change is known. Test data are generated by

$$\phi_k = [\, u_k \quad 1 \,]^T$$
$$u_k = \sin\left(\frac{k}{50}\pi\right)$$
$$y_k = \sum_{i=1}^{2} P_i(\phi_k)\theta_{i,k}^T \phi_k \tag{39}$$

where the input signal is given by a sinusoidal signal. $\theta_{i,k}$ denotes the parameter of the ith mode at the kth sampling instant. The profiles of time-varying parameters θ and η are shown in Fig. 6 and the output signal is shown in Fig. 7. Here, the output y_k is plotted in red when $P_1(\phi_k) \geq P_2(\phi_k)$ and in blue if otherwise. These colors represent modes 1 and 2, respectively.

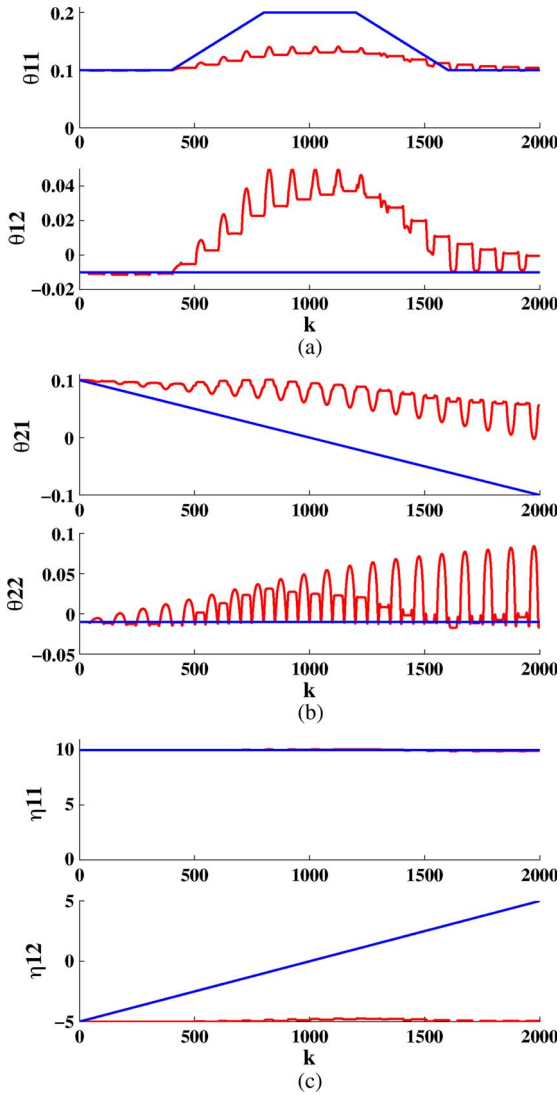

Fig. 8. Profiles of identified and true parameters ($\tau = 1$).

We have analyzed the online estimation under three different conditions of $\tau = 1, 50,$ and 100. Figs. 8–10 show the time series of true (blue) and estimated (red) parameters. Figs. 11–13 show the time series of the output error of the estimated models.

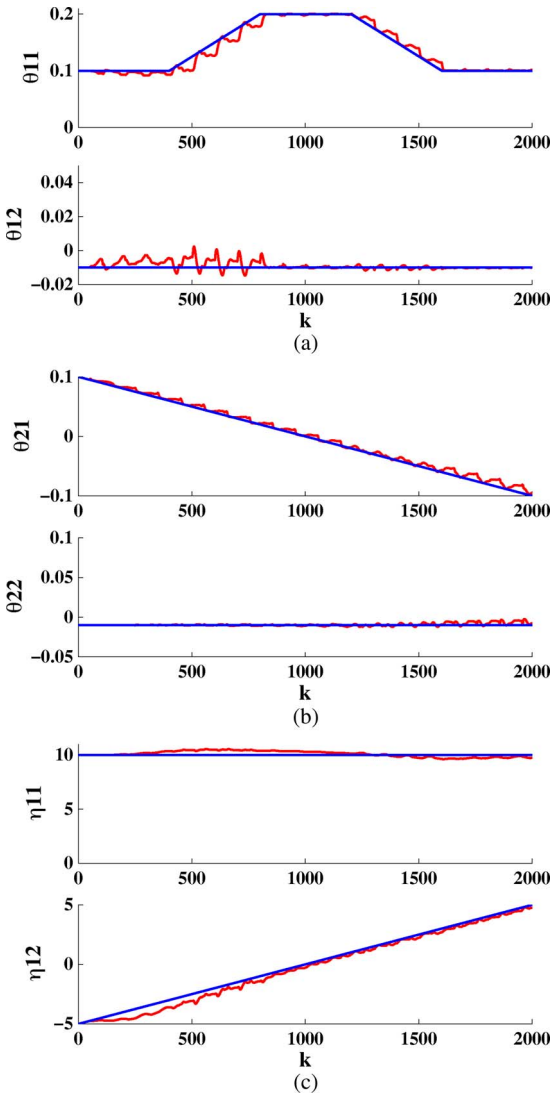

Fig. 9. Profiles of identified and true parameters ($\tau = 50$).

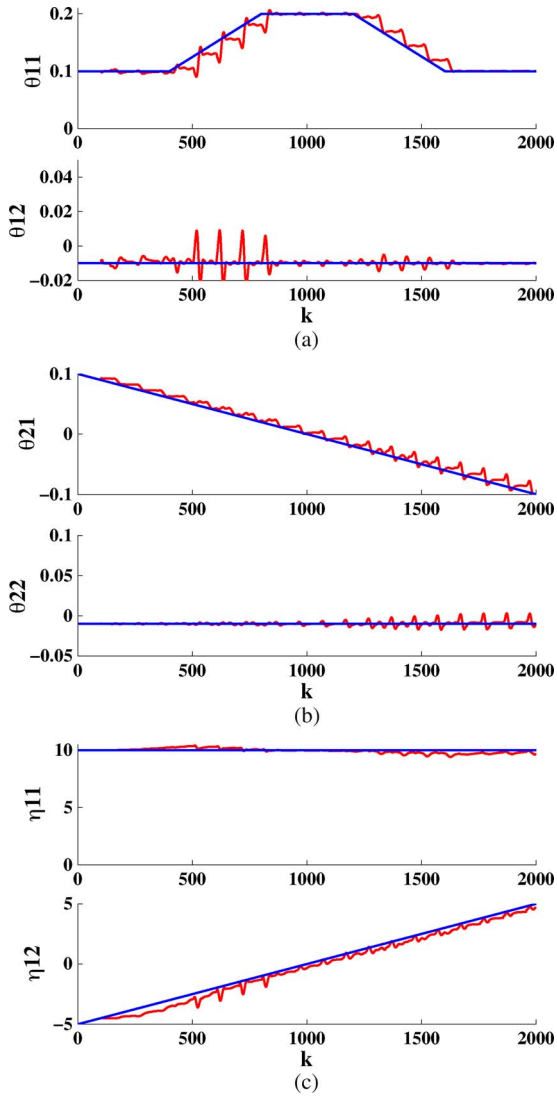

Fig. 10. Profiles of identified and true parameters ($\tau = 100$).

As shown in Fig. 8, the proposed estimation is not able to follow the change of the true parameters in the case of $\tau = 1$. In particular, the estimated value of the mode segmentation parameter η remains almost unchanged. In the case of $\tau = 50$, on the other hand, the adaptive method is able to follow the change of the true parameters, as shown in Fig. 9. In the case of $\tau = 100$, the adaptive method is mostly able to follow the true parameters but with a slightly worse accuracy value than the case of $\tau = 50$.

Next, the results are compared in terms of the output error, i.e., the difference between the output of the original true model and that of the identified model. In the case of $\tau = 1$, a large output error is observed, particularly when the mode transition occurs. This is because τ is too small to acquire enough information on the mode switching, which is necessary for estimating η. In the case of $\tau = 100$, the result shows larger output error compared with the case of $\tau = 50$. This is also emphasized when θ is changing. This happens because the value of τ is so large that the estimated parameters are influenced by data in the past.

Finally, other different values of τ are compared in terms of the mean square error of the model output and the model

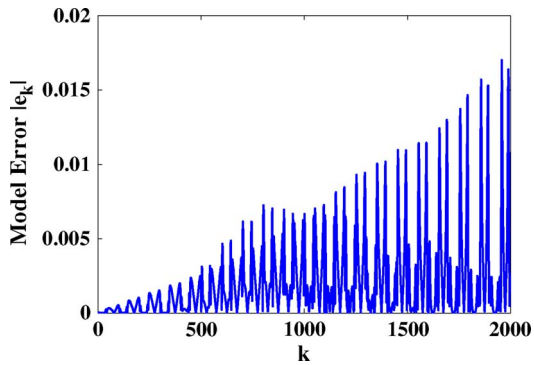

Fig. 11. Profile of output error ($\tau = 1$).

parameters. The results are summarized in Figs. 14 and 15. As shown in Fig. 14, the output error becomes the smallest when $\tau = 10$. This result shows that the smaller the data length is, the more accurately the model reproduces the original data unless τ takes an excessively small value such as $\tau = 1$. Fig. 15, on the other hand, shows that the mean square error between the estimated and the true parameters becomes the smallest when $\tau = 60$. As the reason for this, it can be pointed out that the in-

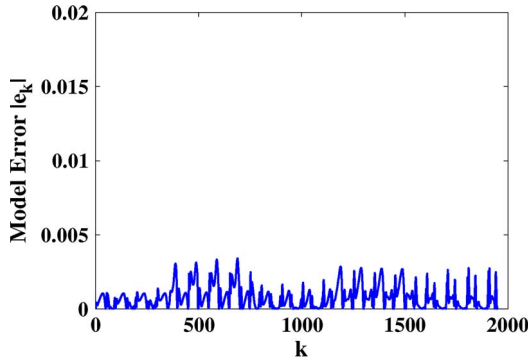

Fig. 12. Profile of output error ($\tau = 50$).

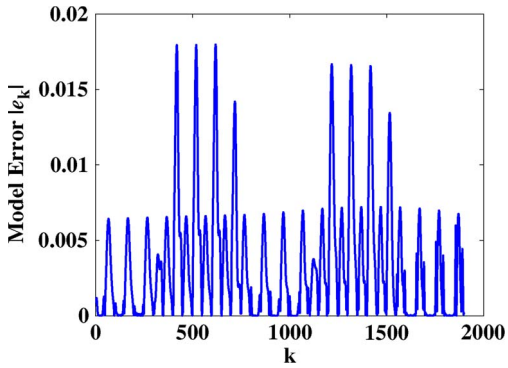

Fig. 13. Profile of output error ($\tau = 100$).

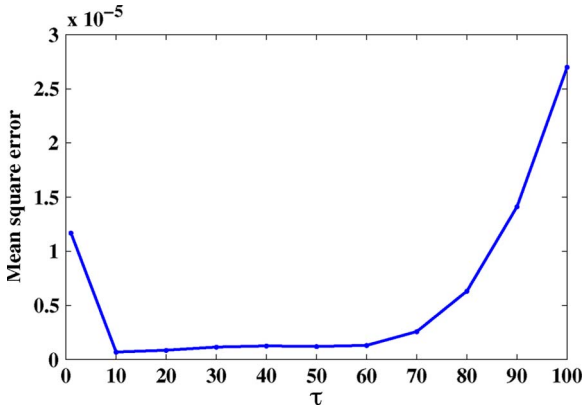

Fig. 14. Mean square error of outputs for various τ

terval of mode transition for the true parameters is 50–60 steps (see Fig. 7). From these discussions, we can conclude that the data length τ should be set as small as possible under the condition that it is greater than the average period of mode transition.

III. Analysis and Modeling of Driving Behavior

Human behavior can be considered to consist of the function of decision-making and motion control. The former can be characterized by logical switching, whereas the latter can be described by continuous dynamics. Therefore, by applying the hybrid system identification to the human behavioral data, it is expected to simultaneously extract the decision-making and motion-control aspects from the observed behavioral data.

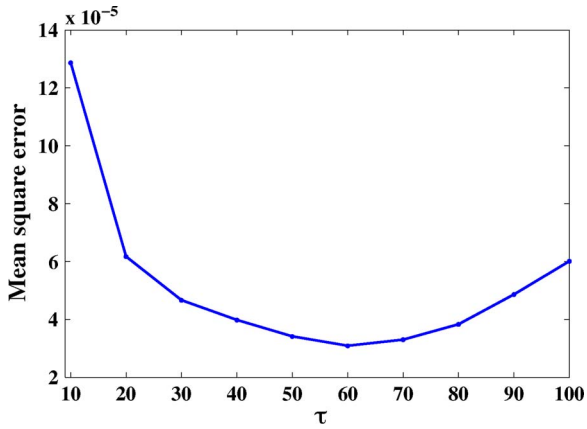

Fig. 15. Mean square error of parameters for various τ.

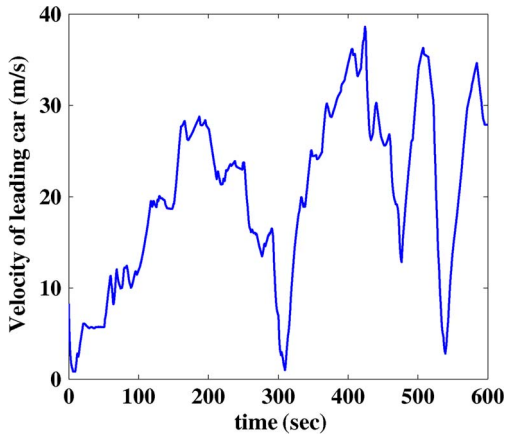

Fig. 16. Velocity pattern of a leading vehicle.

Here, the proposed PrARX model is applied to the analysis of the driving behavioral data. The estimated θ and η in the identified PrARX model are expected to represent the motion-control and decision-making aspects of the driver, respectively. The usefulness of the proposed PrARX model is also verified.

A. Acquisition of Driving Data

The driving data are acquired though a driving simulator that provides an immersive environment. In this paper, we focus on the driver's vehicle-following task on an expressway. The leading vehicle departs 30[m] ahead and runs at a velocity pattern shown in Fig. 16. All drivers are instructed to follow the leading car in their usual manner. The view from the driver is shown in Fig. 17.

B. Definition of Driver Input and Output

The driver's input and output variables are defined as follows:

Input variables

- u_1: Risk-feeling index KdB
- u_2: Range (relative distance between cars) [m]
- u_3: Range rate (relative velocity between cars) [m/s]

Output variable

- y: Acceleration $[\mathrm{m/s}^2]$

Fig. 17. Driver's view in the driving simulator.

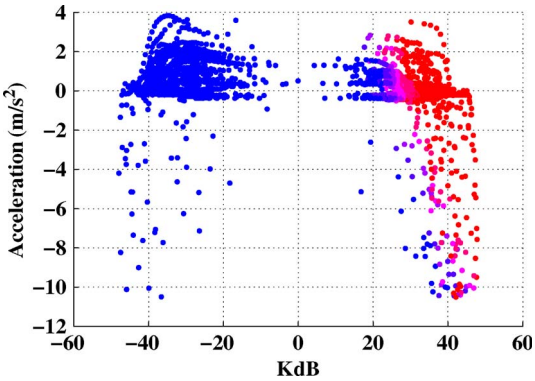

Fig. 18. Mode-segmentation result of the vehicle-following task (driver A; two-mode model, KdB–acceleration).

KdB is a risk-feeling index defined as the logarithm of the time derivative of the leading vehicle's back area projected onto the driver's retina [19]. The KdB can be expressed by using u_2 and u_3 as follows:

$$u_1 = \begin{cases} 10 \times \log(-\kappa), & \text{if } \kappa < -1 \\ -10 \times \log(\kappa), & \text{if } \kappa > 1 \\ 0, & \text{if } -1 \leq \kappa \leq 1 \end{cases} \tag{40}$$

where κ is defined by

$$\kappa = 4 \times 10^7 \times \frac{u_3}{{u_2}^3}. \tag{41}$$

Intuitively speaking, the larger the KdB is, the more dangerous a situation the driver faces. All variables are normalized before identification. The number of modes is set to be 2. Since we consider first-order dynamics as the controller model, the regressor vector $\boldsymbol{r}_k$ is defined as follows:

$$\boldsymbol{r}_k = [y_{k-1}\ u_{1,k-1}\ u_{2,k-1}\ u_{3,k-1}]^T. \tag{42}$$

C. Modeling Results

1) Mode-Segmentation Results: First, the driver model is identified by using 2434 points of data. The mode-segmentation results in the KdB–acceleration space in the case of the two-mode modeling of the drivers A and B are shown in Figs. 18 and 19, respectively. In these figures, the red and blue markers show the corresponding modes. (The color is changed gradually based on probability.) The dangerous region, where the range

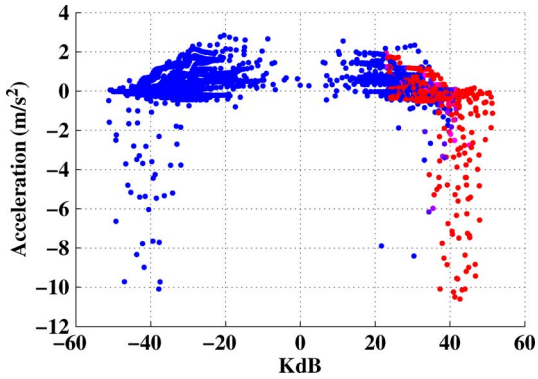

Fig. 19. Mode-segmentation result of vehicle-following task (driver B; two-mode model, KdB–acceleration).

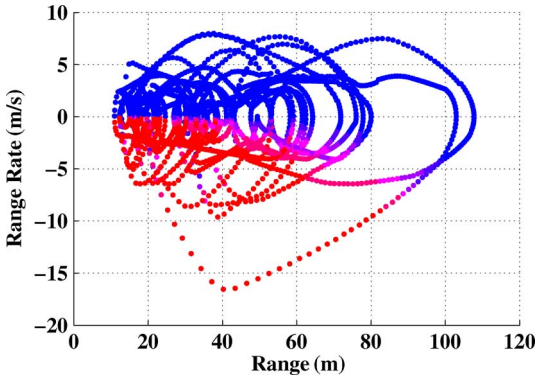

Fig. 20. Mode segmentation result of the vehicle-following task (driver A; two-mode model, range–range rate).

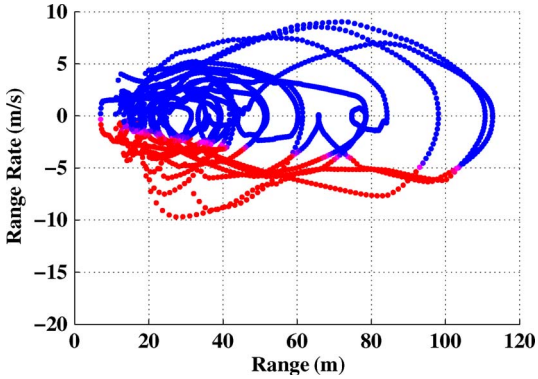

Fig. 21. Mode-segmentation result of the vehicle-following task (driver B, two-mode model, range–range rate).

is small and the range rate is largely negative, is indicated by the red mode. Figs. 20 and 21 show the mode-segmentation results in the range–range rate space. In addition, Figs. 22 and 23 show the mode-segmentation results in the KdB–range space. In these figures, we can see that the braking operation is activated many times in the red mode, and that the red mode appears on the region where the KdB is large. This implies that the KdB strongly affects the mode segmentation, i.e., the decision-making of the driver. This point can also be verified by investigating the magnitude of the parameters η_1, which is addressed in Section III-C3. In addition, the three-mode model and the four-mode model are applied to the same data. Fig. 24 shows the mean square error for various models. From

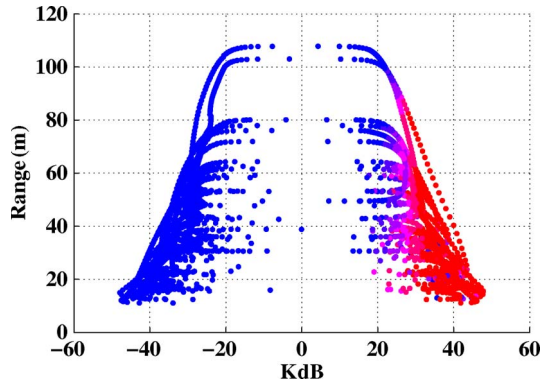

Fig. 22. Mode-segmentation result of the vehicle-following task (driver A; two-mode model, KdB–range).

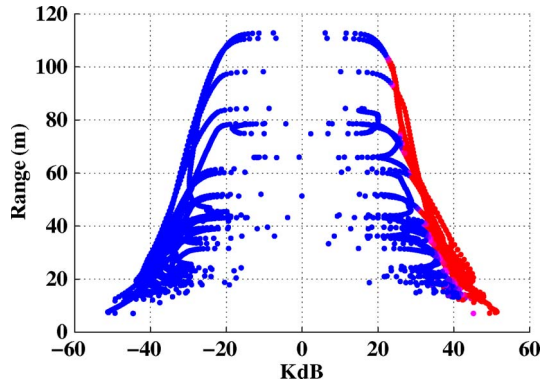

Fig. 23. Mode-segmentation result of the vehicle-following task (driver B; two mode model, KdB–range).

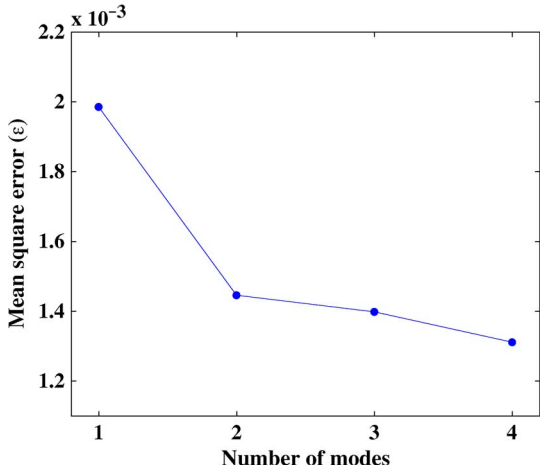

Fig. 24. Mean square error for various number of modes.

this figure, the mean square error of the two-mode model is similar to that of the three-mode mode model and that of the four-mode model. Generally speaking, it is desirable that the number of modes is as small as possible from the viewpoint of computational complexity. In addition, the difference of the mean square error between the single-mode model and the two-mode model is much larger than that between the two-mode model and the three-mode model. Therefore, we can conclude that the optimal number of the modes is two. In the remaining part of this paper, the two-mode model is analyzed.

TABLE I
IDENTIFIED PARAMETERS $\boldsymbol{\theta}_i$

Driver	mode (i)	θ_{i1}	θ_{i2}	θ_{i3}	θ_{i4}	θ_{i5}
A	1	0.910	-0.170	0.152	0.251	0.105
	2	0.801	-0.048	0.061	0.030	-0.041
B	1	0.902	-0.113	0.114	0.080	0.050
	2	0.733	-0.005	0.039	-0.002	-0.005
C	1	0.855	-0.129	0.126	0.134	0.069
	2	0.750	-0.011	-0.040	0.012	-0.009
D	1	0.942	0.064	0.044	0.046	-0.042
	2	0.869	0.119	-0.042	0.010	0.083
E	1	0.966	-0.119	0.138	0.229	0.056
	2	0.753	-0.098	-0.124	0.148	-0.039

TABLE II
IDENTIFIED PARAMETERS $\boldsymbol{\eta}_1$

Driver	η_{11}	η_{12}	η_{13}	η_{14}	η_{15}
A	8.661	13.059	-7.500	-10.522	-4.869
B	-13.242	27.785	-8.992	-51.645	-28.622
C	-4.628	20.931	-28.774	-8.151	-2.943
D	-0.002	4.484	0.035	-2.263	0.976
E	0.017	3.520	-0.161	-0.748	0.336

2) Identified Parameters $\boldsymbol{\theta}_i$: The identified $\boldsymbol{\theta}_i$ values in the PrARX model are shown in Table I. In this table, modes 1 and 2 mean the red and blue modes in Figs. 20 and 21, respectively. The coefficient of the autoregressive term θ_{i1} takes a smaller value in mode 2 than in mode 1. This implies that the driver shows faster dynamics in mode 2 than in mode 1. In addition, the other parameters θ_{i2}, θ_{i3}, and θ_{i4} tend to be larger in mode 1 than in mode 2. This implies that the driver uses higher gain feedback control in mode 1.

3) Identified Parameters $\boldsymbol{\eta}_1$: The identified $\boldsymbol{\eta}_1$ values in the PrARX model are shown in Table II. Note that $\boldsymbol{\eta}_2 = 0$ according to definition of the PrARX model. The probability that the $\boldsymbol{r}_k$ belongs to the corresponding mode can be calculated by these parameters. The matrix H_i that specifies the region of each mode are calculated by using (16) and is given by

$$\boldsymbol{H}_1 = \begin{bmatrix} (\boldsymbol{\eta}_1 - \boldsymbol{\eta}_1) \\ (\boldsymbol{\eta}_2 - \boldsymbol{\eta}_1) \end{bmatrix} = \begin{bmatrix} \boldsymbol{0} \\ -\boldsymbol{\eta}_1 \end{bmatrix} \tag{43}$$

$$\boldsymbol{H}_2 = \begin{bmatrix} (\boldsymbol{\eta}_1 - \boldsymbol{\eta}_2) \\ (\boldsymbol{\eta}_2 - \boldsymbol{\eta}_2) \end{bmatrix} = \begin{bmatrix} \boldsymbol{\eta}_1 \\ \boldsymbol{0} \end{bmatrix}. \tag{44}$$

Then, the deterministic partition between modes 1 and 2 is given by

$$\boldsymbol{\eta}_1^T \boldsymbol{\varphi} = 0. \tag{45}$$

Therefore, the large element in the η indicates that it strongly affects the partition between modes, i.e., the driver's decision-making. In Table II, it can be seen that the KdB and the range rate have strong influences on the decision-making of the driver A. Similarly, the KdB and the range have a strong influence on the decision-making of driver B. Generally speaking, the KdB has the strong influence on the decision-making. The parameter $\boldsymbol{\eta}_1$ can be an important feature value to design the assisting system that accommodates with each driver's personality.

TABLE III
COMPARISON OF MEAN SQUARE ERROR

Driver	PrARX	PWARX
A	0.0007	0.0009
B	0.0019	0.0024
C	0.0020	0.0025
D	0.0018	0.0022
E	0.0027	0.0049
ALL	0.0019	0.0024

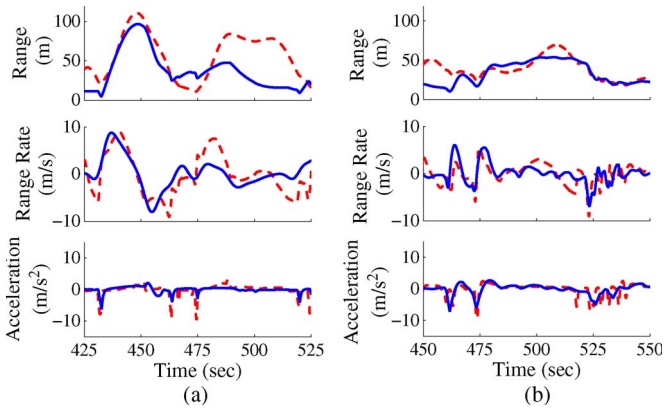

Fig. 25. Comparison of the calculated closed-loop behavior (blue solid lines) with the observed behavior (red dashed lines).

4) Modeling Accuracy: The output error of the PrARX model is compared with that of the PWARX model, which is identified by using the clustering-based approach [14]. The mean square errors are shown in Table III. In this table, the PrARX model shows better modeling accuracy than the PWARX model.

5) Verification by Closed-Loop Behavior: Next, the modeling accuracy of the identified model is verified again by calculating the closed-loop behavior wherein the identified driver model is embedded together with the vehicle model. This verification is carried out by the following procedure.

Step 1: States (positions, velocity, and acceleration of the own car and the leading car) are initialized.
Step 2: The input data of the driver model (KdB, range, and range rate) are calculated based on the states.
Step 3: The output (acceleration of own car) is calculated using the identified driver model.
Step 4: The states of the cars are updated based on the vehicle model with the obtained acceleration and the velocity pattern of the leading car.
Step 5: Go to Step 2.

We could verify that the car kept following the leading car without any collision with the leading car or getting far from the leading car. Enlarged profiles of the comparison between the calculated closed-loop behavior using the driver model (blue solid line) and the observed behavior (red dashed line) are shown in Fig. 25. It is found that the closed-loop behavior and the observed behavior agrees well with each other in these figures. In particular, we can find the coincidence of the changes of the acceleration in both drivers. Thus, it is confirmed that the original behavior is well reproduced by the identified model.

TABLE IV
DECISION ENTROPY

Driver	A	B
Entropy	379.3873	116.3629

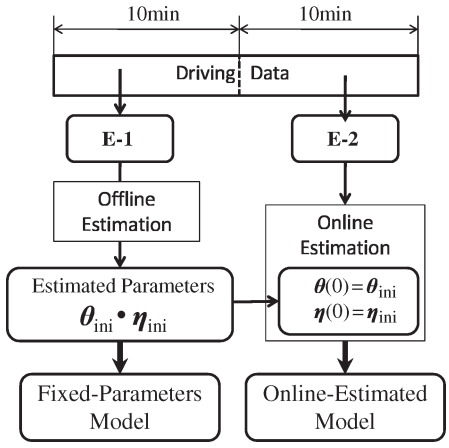

Fig. 26. Procedure of the experiment.

D. Decision Entropy

By using the PrARX model, the "decision entropy" can be defined, which is a quantitative measure to evaluate the vagueness of the decision-making. Decision entropy is defined as follows:

$$H(P_i) = \int_{\boldsymbol{r}\in D_H} \sum_{i=1}^{s} P_i \log(P_i)\, d\boldsymbol{r} \tag{46}$$

where D_H is the region of the collected regressor vector. The larger the decision entropy is, the more the vagueness in the decision-making is. The calculated decision entropy of drivers A and B is shown in Table IV. In this table, the decision entropy of driver A is less than that of driver B. This implies that the decision-making of driver B is more unclear than that of driver A. This can also be verified by comparing Figs. 20 and 21. The unclear region (between the red mode and the blue mode) of driver B is larger than that of driver A.

E. Adaptive Parameter Estimation

1) Procedure of the Experiment: The proposed adaptive estimation scheme is verified by the following procedure (see also Fig. 26).

Step 1: Each driver executes the vehicle-following task in two successive trials, with 10 min per trial. The data set acquired in the first and second trials are denoted by E-1 and E-2, respectively.
Step 2: Using E-1, model parameters are estimated using offline estimation and denoted by $\theta_{\rm ini}$ and $\eta_{\rm ini}$.
Step 3: Apply the online estimation method to the data set E-2, using $\theta_{\rm ini}$ and $\eta_{\rm ini}$ as the initial parameters.
Step 4: Compare the modeling accuracy of the online-estimated model with that of the fixed-parameter model whose parameters are fixed in $\theta_{\rm ini}$ and $\eta_{\rm ini}$.

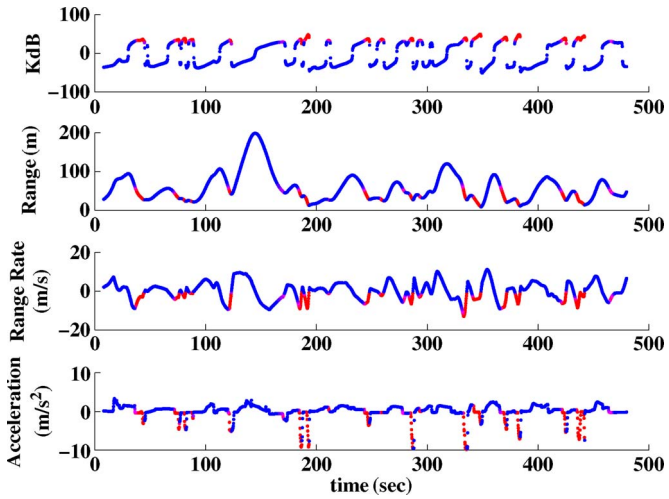

Fig. 27. Time-series data in the E-1 of driver A together with mode segmentation.

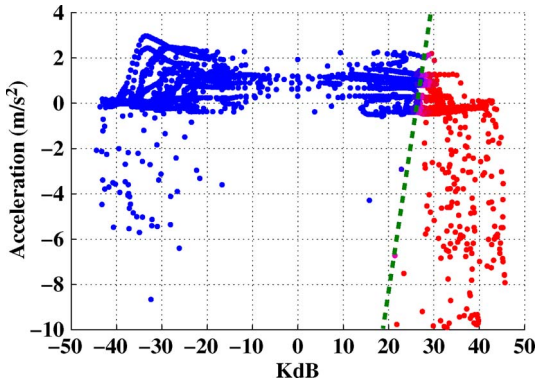

Fig. 28. Mode segmentation as a result of offline estimation (driver A).

Fig. 27 shows the time series data together with the estimated mode (designated by color) in the E-1 (offline estimation) of the driver A. In Fig. 27, we can see that the mode transition between modes 1 and 2 occurs approximately every 40 s, which corresponds to 200 steps. Therefore, based on the discussion in Section II-E, we set the data length of the online estimation, which is the variable parameter depending on the driving situation to be $\tau = 200$. The duration τ should be decided considering the speed of the environment dynamics, such as the velocity profile of the leading car. From the application viewpoint, this duration must be changed according to the traffic density of the road.

2) Results and Analysis: First, the driver model is identified by using an offline estimation. The mode segmentation result in the case of the two-mode modeling of driver A is shown in Fig. 28. In this figure, the collected driving data are plotted in the KdB–acceleration space. The colors of each data are defined according to the mode probability. The meaning of color is the same as in Figs. 18 and 19.

Next, the data set E-2 of the same driver is analyzed using online estimation. Figs. 29 and 30 show the mode segmentation result of the online estimation after 100 and 400 s, respectively. The profiles of the estimated parameters θ and η are shown in Figs. 31–33, respectively. When we look at Figs. 29 and 30, we can see that the region of mode 1 shrinks gradually

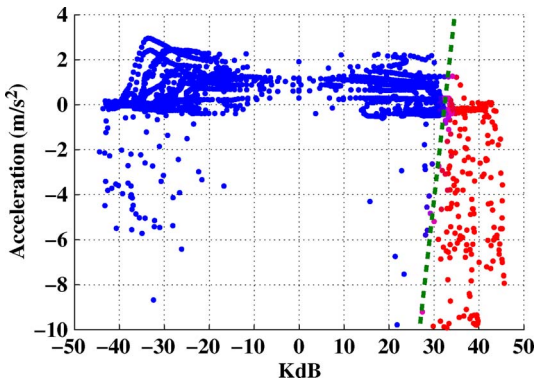

Fig. 29. Mode segmentation as a result of online estimation (driver A; after 100 s).

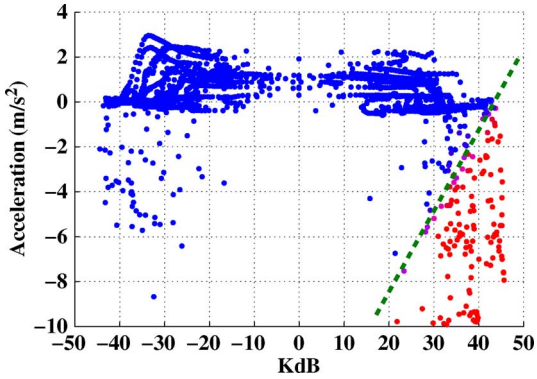

Fig. 30. Mode segmentation as a result of online estimation (driver A; after 400 s).

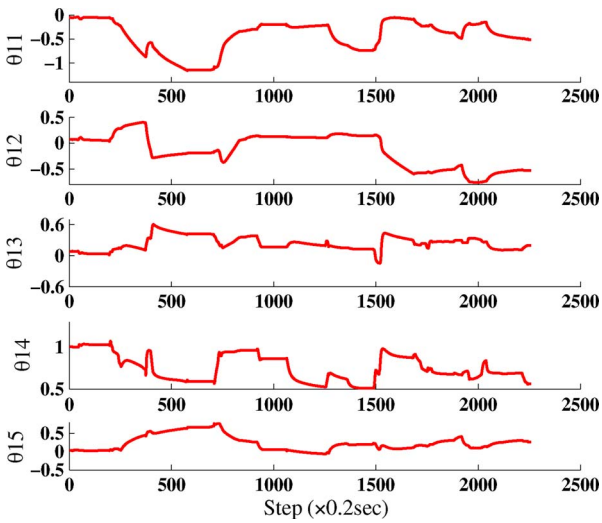

Fig. 31. Profile of identified parameter θ_1.

according to the progress of the execution time. The reason for this shrinking is considered to be that the driver can adapt to both the driving situation and the equipment installed in the driving simulator after a certain time of driving. As a result, the driver becomes more insensitive to the risk of collision, i.e., becomes less likely to switch to the collision-avoidance mode. This also can be validated by the profiles shown in Figs. 34 and 35, which represent the slope and the constant term of the separating hyperplane between modes 1 and 2, respectively (denoted by the green dashed line in Figs. 29 and 30). We can

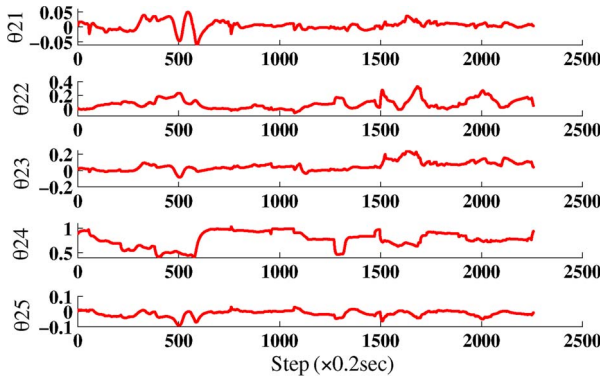

Fig. 32. Profile of identified parameter θ_2.

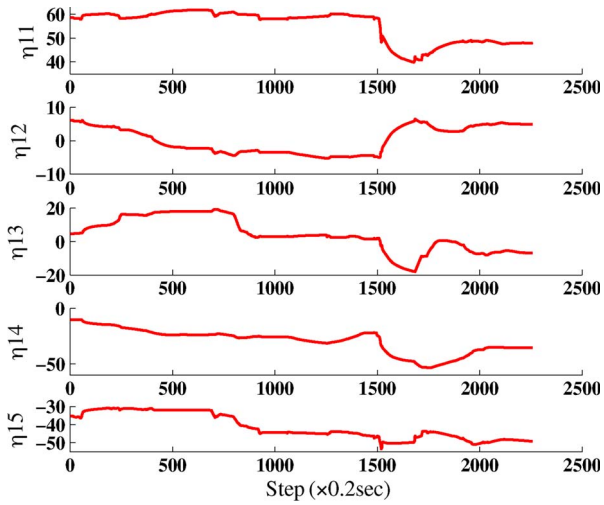

Fig. 33. Profile of identified parameter η_1.

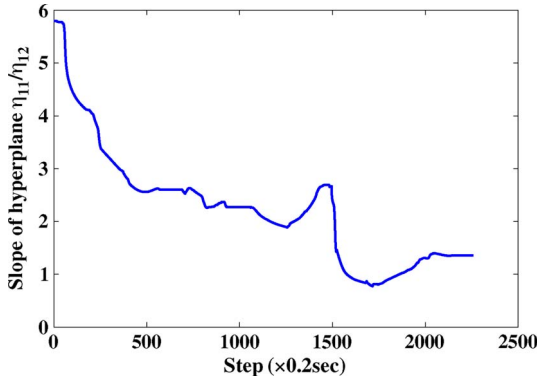

Fig. 34. Profile of η_{11}/η_{12}.

see that the slope decreases and the constant term increases according to progress of the time. Note that the small peak around 1500 steps (300 s) in Fig. 34 is caused by the stop of the leading vehicle (see also Fig. 16). Although the motion-control parameter θ sometimes shows an abrupt change due to the abrupt change of the driving situation (Figs. 31 and 32), the decision-making parameter η seldom shows a sudden change even in such a case (see Fig. 33). This coincides well with our intuitive understanding of the human behavior.

Finally, we compare the adaptive estimation with fixed estimation in terms of modeling accuracy.

Table V shows the comparison of the mean square output error of the five examinees in the cases of the fixed-parameter

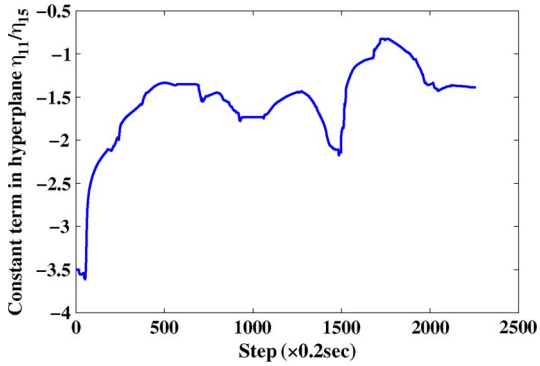

Fig. 35. Profile of η_{11}/η_{15}.

TABLE V
COMPARISON OF OUTPUT ERROR BETWEEN ADAPTIVE AND FIXED ESTIMATIONS

driver	Adaptive	Fixed
A	0.0024	0.0139
B	0.0011	0.0102
C	0.0030	0.0126
D	0.0109	0.0321
E	0.0008	0.0057

estimation and the adaptive parameter estimation. In this table, the adaptive estimation shows better modeling accuracy than the fixed-parameter model.

Note that in these experiments, the computation time required for online estimation is shorter than the sampling interval (200 ms). Therefore, the proposed algorithm can be exploited for the real-time assisting control.

IV. DISCUSSION

The useful features of the proposed PrARX model are summarized as follows.

- In the understanding of the complex physical phenomena, such as human behavior or the biological system, the probabilistic partition may fit well due to the continuity underlying the original phenomena. In these application fields, the modeling error tends to be smaller than the PWARX model that has the deterministic partition since the PrARX model can represent the composition of several modes. Furthermore, the stochastic characteristics of the partition may represent some important factor in the original phenomena such as decision entropy.
- The identification scheme of the PrARX model can be exploited as the identification scheme of the PWARX model by applying simple transformation rule. From the viewpoint of the identification strategy of the PWARX model, the proposed identification scheme can realize the simultaneous estimation of the parameters in the ARX models and in the partitions by a single optimization. Furthermore, the obtained parameters give a complete partition.
- Due to the simple parameter-estimation algorithm with small computational cost, it can be easily extended to the adaptive parameter-estimation scheme, which can update the estimated parameters online. As a result, the model can adapt to changes in the driving characteristics.

V. Conclusion

In this paper, we have proposed a PrARX model wherein the multiple ARX models are composed by the probabilistic weighting functions. As the probabilistic weighting function, the "softmax" function was exploited. Then, the parameter-estimation problem for the proposed model was formulated as a single optimization problem, and the estimation algorithm was derived. Since the PrARX model can represent both motion control and decision-making aspects in human driving behavior, it can be one of the promising mathematical driving behavior models. Through application of the vehicle-following behavior, the risk-feeling factor has been found to play an essential role in a driver's decision-making to switch the control law from the following mode to the collision-avoidance mode. In addition, decision entropy that represents the vagueness of the human driver has been quantitatively defined. This measure can reflect the performance of the human driver from the viewpoint of the decision-making.

The most promising application of the proposed driving behavior model is a systematic design of the personalized driver-assisting system. Due to the explicit representation of both motion control and decision-making aspects in the PrARX model, it leads to the development of a so-called model predictive control, wherein the driving behavior model of individual drivers is explicitly included. In addition, there are many demands for the quantitative evaluation of the decision-making of the driver. The typical application is to test the human–machine interface (HMI) in the vehicle. The conventional testing methods for the HMI (occlusion test and so on) focus only on the evaluation of the usability of the device itself. The proposed decision entropy will provide us with a new index for the evaluation of the HMI from the viewpoint of safe driving.

Furthermore, the online parameter-estimation method for the PrARX model has been developed to overcome the problem that the dynamical characteristics of the driving behavior changes. The proposed online scheme has been developed based on an assumption that human driving behavior gradually changes with a sufficiently slow speed. This assumption, however, seems quite reasonable because it is likely that the dynamic characteristics of the human driving behavior discontinuously and instantaneously change in the safe-driving situation. The proposed method has also been applied to the modeling of the vehicle-following behavior, and it has been found that the driver's risk feeling goes down as time progresses. This was most likely caused by the accommodation of the driver with the driving situation.

Generally speaking, it seems to be quite difficult to collect enough driving data in advance. The proposed framework can overcome this problem by adapting the initial parameters of the model to the updated data set in real time. This advantage also gives us a solution for capturing the change of the driving characteristics of the driver caused by the driving experience and/or the fatigue by long driving. In other words, the proposed model can be used as a kind of sensor to detect the driver's internal state by looking at the change of the parameters of the identified model in real time. This "virtual sensor" will be exploited for the design of the warning system to prevent the accident caused by drowsiness and/or distraction.

References

[1] D. McRuer and D. Weir, "Theory of manual vehicular control," *Ergonomics*, vol. 12, no. 4, pp. 599–633, Jul. 1969.

[2] C. MacAdam, "Application of an optimal preview control for simulation of closed-loop automobile driving," *IEEE Trans. Syst., Man, Cybern.*, vol. SMC-11, no. 9, pp. 393–399, Jun. 1981.

[3] A. Modjtahedzadeh and R. Hess, "A model of driver steering control behavior for use in assessing vehicle handling qualities," *ASME J. Dyn. Syst. Meas. Control*, vol. 15, no. 3, pp. 456–464, Sep. 1993.

[4] T. Pilutti and A. G. Ulsoy, "Identification of driver state for lane-keeping tasks," *IEEE Trans. Syst., Man, Cybern. A, Syst., Humans*, vol. 29, no. 5, pp. 486–502, Sep. 1999.

[5] S. D. Keen and D. J. Cole, "Bias-free identification of a linear model-predictive steering controller from measured driver steering behavior," *IEEE Trans. Syst., Man, Cybern. B, Cybern.*, vol. 42, no. 2, pp. 434–443, Apr. 2012.

[6] P. Angkititrakul, C. Miyajima, and K. Takeda, "Modeling and adaptation of stochastic driver-behavior model with application to car following," in *Proc. IEEE IV*, 2011, pp. 814–819.

[7] J. Sjoberg, Q. Zhang, L. Ljung, A. Benveniste, B. Deylon, P. Y. Glorenner, H. Hjalmarsson, and A. Juditsky, "Nonlinear black-box modeling in system identification: A unified overview," *Automatica*, vol. 31, no. 12, pp. 1691–1724, Dec. 1995.

[8] K. S. Narendra and K. Pathasarathy, "Identification and control of dynamical systems using neural networks," *IEEE Trans. Neural Netw.*, vol. 1, no. 1, pp. 4–27, Mar. 1990.

[9] M. C. Nechyba and Y. Xu, "Human control strategy: Abstraction, verification, and replication," *IEEE Control Syst.*, vol. 17, no. 5, pp. 48–61, Oct. 1997.

[10] G. S. Aoude, V. R. Desaraju, L. H. Stephens, and J. P. How, "Driver behavior classification at intersections and validation on large naturalistic data set," *IEEE Trans. Intell. Transp. Syst.*, vol. 13, no. 2, pp. 724–736, Jun. 2012.

[11] F. A. Mussa-Ivaldi, S. F. Giszter, and E. BIzzi, "Linear combinations of primitives in vertebrate motor control," *Proc. Nat. Acad. Sci.*, vol. 91, no. 16, pp. 7534–7538, Aug. 1994.

[12] C. Bregler and J. Malik, "Learing and recognizing human dynamics in video sequences," in *Proc. IEEE Conf. Comput. Vis. Pattern Recognit.*, 1997, pp. 568–574.

[13] D. D. Vecchio, R. M. Murray, and P. Perona, "Decomposition of human motion into dynamics-based primitives with application to drawing tasks," *Automatica*, vol. 39, no. 12, pp. 2085–2098, Dec. 2003.

[14] G. Ferrari-Trecate, M. Muselli, D. Liberati, and M. Morari, "A clustering technique for the identification of piecewise affine system, automatica," *Automatica*, vol. 39, no. 2, pp. 205–217, Feb. 2003.

[15] E. Amaldi and M. Mattavelli, "The MIN PFS problem and piecewise linear model estimation," *Discrete Appl. Math.*, vol. 118, no. 1/2, pp. 115–143, Apr. 2002.

[16] J. Roll, A. Bemporad, and L. Ljung, "Identification of piecewise affine systems via mixed-integer programming," *Automatica*, vol. 40, no. 1, pp. 37–50, Jan. 2004.

[17] A. Bemporad, A. Garulli, S. Paoletti, and A. Vicino, "A bounded-error approach to piecewise affine system identification," *IEEE Trans. Autom. Control*, vol. 50, no. 10, pp. 1567–1580, Oct. 2005.

[18] A. Juloski and S. Weiland, "A Bayesian approach to the identification of piecewise linear output error models," in *Proc. 14th IFAC Symp. Syst. Identification*, Newcastle, Australia, 2006, pp. 374–379.

[19] T. Wada, S. Doi, K. Imai, N. Tsuru, K. Isaji, and H. Kaneko, "Analysis of drivers' behaviors in car following based on a performance index for approach and alienation," presented at the Soc. Autom. Eng. World Congr., Detroit, MI, 2007, Paper 2007-01-0440.

[20] J. H. Kim, S. Hayakawa, T. Suzuki, K. Hayashi, S. Okuma, N. Tsuchida, M. Shimizu, and S. Kido, "Modeling of driver's collision avoidance maneuver based on controller switching model," *IEEE Trans. Syst., Man, Cybern. B, Cybern.*, vol. 35, no. 6, pp. 1131–1143, Dec. 2005.

[21] S. Sekizawa, S. Inagaki, T. Suzuki, S. Hayakawa, N. Tsuchida, T. Tsuda, and H. Fujinami, "Modeling and recognition of driving behavior based on stochastic switched ARX model," *IEEE Trans. Intell. Transp. Syst.*, vol. 8, no. 4, pp. 593–606, Dec. 2007.

[22] T. Akita, T. Suzuki, S. Hayakawa, and S. Inagaki, "Analysis and synthesis of driving behavior based on mode segmentation," in *Proc. Int. Conf. Control, Autom. Syst.*, 2008, pp. 2884–2889.

Hiroyuki Okuda was born in Gifu, Japan, in 1982. He received the B.E. and M.E. degrees in advanced science and technology from Toyota Technological Institute, Nagoya, Japan, in 2005 and 2007, respectively, and the Ph.D. degree in mechanical science and engineering from Nagoya University, in 2010.

From 2010 to 2012, he was a Postdoctoral Researcher with the Core Research for Evolutional Science and Technology, Japan Science and Technology Agency. He is currently an Assistant Professor with the Green Mobility Collaborative Research Center, Nagoya University. His research interests include system identification of hybrid dynamical system and its application to modeling of human behavior, design of human-centered mechatronics, and biological signal processing.

Dr. Okuda is a member of the Institute of Electrical Engineers of Japan, the Society of Instrument and Control Engineers, and the Japan Society of Mechanical Engineers.

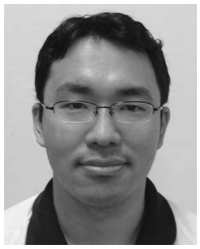

Norimitsu Ikami was born in Aichi, Japan, in 1987. He received the B.E. degree from Nagoya University, Nagoya, Japan, in 2010. He is currently workting toward the Master's degree with the Department of Mechanical Science and Engineering, Nagoya University.

His research interests include modeling and analysis of human driving behavior, and the design of driving assist systems.

Tatsuya Suzuki (M'91) was born in Aichi, Japan, in 1964. He received the B.S., M.S., and Ph.D. degrees from Nagoya University, Nagoya, Japan, in 1986, 1988, and 1991, respectively, all in electronic mechanical engineering.

From 1998 to 1999, he was a Visiting Researcher with the Department of Mechanical Engineering, University of California, Berkeley. He is currently a Professor with the Department of Mechanical Science and Engineering, Nagoya University. His current research interests include hybrid dynamical systems and discrete event systems, particularly focusing on the application to human behavior analysis and dependable mechatronics design.

Dr. Suzuki is a member of the Institute of Electronics, Information and Communications Engineers, the Japan Society of Automotive Engineers, the Robotics Society of Japan, the Japan Society of Mechanical Engineers, and the Institute of Electrical Engineers of Japan. He received the Outstanding Paper Award at the 2008 International Conference on Control Automation and Systems and the Journal Paper Award from SICE and JSAE in 2009 and 2010, respectively.

Yuichi Tazaki (M'08) was born in Kanagawa, Japan, in 1980. He received the Dr.Eng degree in control engineering from Tokyo Institute of Technology, Tokyo, Japan, in 2008.

From 2007 to 2009, he was a Research Fellow with the Japan Society for the Promotion of Science, Tokyo. In 2008, he was a Guest Scientist with Honda Research Institute Europe, Offenbach, Germany. Since 2009, he has been an Assistant Professor with Nagoya University, Nagoya, Japan. His research interests include abstraction and control of hybrid systems, control of bipedal robots, and motion planning of humanoid robots.

Mr. Tazaki is a member of the Society of Instrument and Control Engineers, and The Robotics Society of Japan.

Kazuya Takeda (SM'09) received the B.E. and M.E. degrees in electrical engineering and the Doctor of Engineering degree from Nagoya University, Nagoya, Japan, in 1983, 1985, and 1994, respectively.

From 1986 to 1989, he was with the Advanced Telecommunication Research Laboratories (ATR), Osaka, Japan. His main research interest at ATR was corpus-based speech synthesis. From November 1987 to April 1988, he was a Visiting Scientist with the Massachusetts Institute of Technology, Cambridge. From 1989 to 1995, he was a Researcher and Research Supervisor with KDD Research and Development Laboratories, Kamifukuoka, Japan. From 1995 to 2003, he was an Associate Professor with the Faculty of Engineering, Nagoya University. Since 2003, he has been a Professor with the Department of Media Science, Graduate School of Information Science, Nagoya University. He is the author or coauthor of more than 100 journal papers, six books, and more than 100 conference papers. His current research interests include media signal processing and its applications, including spatial audio, robust speech recognition, and driving behavior modeling.

Dr. Takeda was a Conference Technical Cochair of the 2007 International Conference on Multimodal Interfaces and of the 2009 International Conference on Vehicular Safety and Electronics. He was a Cofounder of the biennial Digital Signal Processing Workshop for In-Vehicle Systems and Safety in 2003.